Structural basis for Rab11-dependent membrane recruitment of a family of Rab11-interacting protein 3 (FIP3)/Arfophilin-1

Tomoo Shiba*†, Hiroshi Koga‡, Hye-Won Shin‡, Masato Kawasaki*, Ryuichi Kato*, Kazuhisa Nakayama‡, and Soichi Wakatsuki*§

*Structural Biology Research Center, Photon Factory, Institute of Materials Structure Science, High Energy Accelerator Research Organization, Tsukuba, Ibaraki 305-0801, Japan; and ‡Graduate School of Pharmaceutical Sciences, Kyoto University, Yoshida-shimoadachi, Sakyo-ku, Kyoto 606-8501, Japan

Edited by Wayne A. Hendrickson, Columbia University, New York, NY, and approved August 22, 2006 (received for review June 26, 2006)

Family of Rab11-interacting protein (FIP)3/Arfophlin-1 and FIP4/Arfophilin-2 are dual effectors for Rab11 and ADP ribosylation factor (ARF)5/ARF6, which are involved in membrane delivery from recycling endosomes to the plasma membrane during cytokinesis. Here, we define the distinct C-terminal binding regions of FIP3 and FIP4 for Rab11 and ARF5/ARF6. Furthermore, we determined the crystal structure of Rab11 in complex with the Rab11-binding domain (RBD) of FIP3. The long amphiphilic α-helix of FIP3-RBD forms a parallel coiled-coil homodimer, with two symmetric interfaces with two Rab11 molecules. The hydrophobic side of the RBD helix is involved in homodimerization and mediates the interaction with the Rab11 switch 1 region, whereas the opposite hydrophilic side interacts with the Rab11 switch 2 and is the major factor contributing to the binding specificity. The bivalent interaction of FIP3 with Rab11 at the C terminus allows FIP3 to coordinately function with other binding partners, including ARFs.

membrane trafficking | Rab–effector complex | x-ray crystallography

Small GTPases belonging to the Ras-like superfamily regulate intracellular membrane trafficking, and ADP ribosylation factor (ARF) and Rab family members participate in multiple stages of trafficking along the exocytic and endocytic pathways. ARF GTPases initiate the budding of coated carrier vesicles by recruiting coat protein complexes onto donor membranes, whereas Rab GTPases regulate the targeting and docking/fusion of vesicles with acceptor membranes (1). Like most GTPases, these proteins cycle between an inactive GDP-bound state and an active GTP-bound state capable of interacting with numerous effector molecules.

In mammals, there are six ARF isoforms that are structurally categorized into three classes: class I, ARF1–ARF3; class II, ARF4 and ARF5; and class III, ARF6 (2). Among these ARFs, those from class I and III are well characterized; ARF1 regulates several aspects of membrane trafficking by recruiting coat proteins and triggering membrane deformation (2), and ARF6 regulates endocytic recycling and actin cytoskeleton remodeling (3). In contrast, little is known about the physiological role(s) of class II ARFs.

The Rab proteins constitute the largest family of small GTPases (>60 members in mammals) (4). Among them, Rab11 is a well characterized regulator of endocytic and recycling pathways. Rab11 associates with a broad range of post-Golgi organelles, including recycling endosomes (5–8), and interacts with several effectors in its GTP-bound state.

Recently, a family of Rab11-interacting proteins (FIPs) has been identified (9–13). FIPs share a highly conserved, ≈20-aa, region termed the Rab11-binding domain (RBD) at their C termini (11, 14). Based on the similarity outside of the RBD, FIPs have been categorized into three classes (14). Members of class I contain a C2 domain (FIP2, Rip11, and RCP), those of class II contain EF hands and a proline-rich region (FIP3/Arfophilin-1/Eferin, and FIP4/Arfophilin-2) (Fig. 7*a*, which is published as supporting information on the PNAS web site), and FIP1, the sole member of class III, lacks any other conserved domains.

The class II FIPs also interact with ARF5 and ARF6 in a GTP-dependent manner (9, 13, 15). Additionally, FIP3 and FIP4 have recently been implicated in the delivery of endosomal vesicles to the cleavage furrow during cytokinesis in conjunction with Rab11 and ARF6 (13, 16–18). To better understand the mechanisms underlying the cross-talk between these GTPases mediated by the class II FIPs, we defined the exact ARF-binding domain (ABD) and RBD of these FIPs. These domains are not overlapping and allow the simultaneous binding of Rab11 and ARF5/ARF6. Furthermore, we determined the crystal structure of the FIP3 RBD in complex with Rab11. The amphiphilic helices from two FIP3-RBD molecules form a coiled-coil homodimer that interacts with two Rab11 molecules. The characteristic structure of the switch 2 region of Rab11, which is highly divergent from the corresponding regions of other Rab proteins, allows its specific interaction with the amphiphilic FIP3-RBD helix.

Results

Delineation of RBD. We first wished to determine the minimal region of class II FIP-RBD. Preliminary yeast two-hybrid analyses revealed that a GTP-bound Rab11 mutant, Q70L, but not a GDP-bound mutant, S25N, interacted with the highly conserved FIP3 and FIP4 C-terminal fragments encompassing residues 607–756 and 484–637, respectively (Fig. 7*b* and data not shown). With this information, we next defined the RBD boundaries by pull-down assays (Fig. 1*a*). FIP3 (residues 607–756) efficiently pulled down Rab11(Q70L) (Fig. 1*a*, lane 3), and truncation of the N-terminal 105 aa (residues 712–756) (Fig. 1*a*, lane 4) or 126 aa (residues 733–756) (Fig. 1*a*, lane 5) did not significantly affect the pull-down efficiency. However, a further truncation of 5 aa (residues 738–756) (Fig. 1*a*, lane 6) dramatically reduced the pull-down efficiency. In striking contrast, truncating only 4 aa from the C terminus (residues 607–752) (Fig. 1*a*, lane 8) completely abrogated Rab11(Q70L) binding. On the basis of these results, we concluded that the minimal RBD of FIP3 encompasses residues 733–756. Essentially the same results were obtained with FIP4, allowing us to conclude that the minimal RBD of FIP4 encompasses residues 613–637 (Fig. 1*b*).

Author contributions: T.S. and H.K. contributed equally to this work; T.S., M.K., R.K., K.N., and S.W. designed research; T.S., H.K., and H.-W.S. performed research; T.S. analyzed data; and T.S., M.K., and K.N. wrote the paper.

The authors declare no conflict of interest.

This article is a PNAS direct submission.

Abbreviations: ARF, ADP ribosylation factor; ABD, ARF-binding domain; FIP, family of Rab11-interacting protein; RBD, Rab11-binding domain; CBB, Coomassie brilliant blue.

Data deposition: The atomic coordinates and structure factors have been deposited in the Protein Data Bank, www.pdb.org (PDB ID code 2D7C).

†Present address: Department of Life Sciences, Graduate School of Arts and Sciences, University of Tokyo, Komaba, Meguro-ku, Tokyo 153-8902, Japan.

§To whom correspondence should be addressed. E-mail: soichi.wakatsuki@kek.jp.

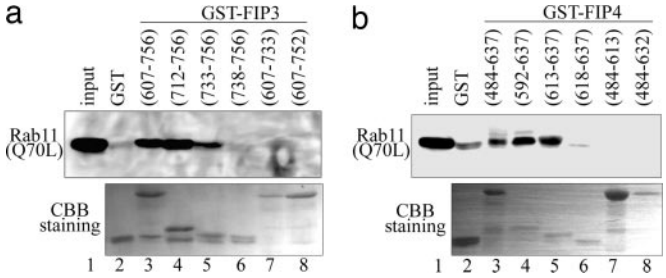

Fig. 1. Delineation of the regions of FIP3 and FIP4 essential for their interactions with Rab11. (*Upper*) Extracts of HeLa cells expressing HA-tagged Rab11(Q70L) were pulled down with GST or FIP3 (*a*) or FIP4 (*b*) GST fusion proteins, as indicated and processed for immunoblot analysis to detect bound HA-Rab11(Q71L). (*Lower*) The blots were then stained with Coomassie brilliant blue (CBB).

FIP3 and FIP4 Bind ARF5/ARF6 by Means of a Region Outside the RBD. Two groups (9, 15) previously reported that both FIP3 and FIP4 can interact with ARFs; yet there were subtle differences between these studies. Exton and colleagues (9, 15) showed that FIP3 interacts with GTP-bound ARF5 and ARF6, whereas Gould and colleagues (13) reported that FIP3 interacts with ARF5, but only very weakly with ARF6, and that FIP4 interacts exclusively with ARF5. We wished to clarify this issue. As shown in Fig. 2*a*, the GTP-bound ARF mutants, ARF5(Q71L) and ARF6(Q67L), were pulled down with GST–FIP3 (residues 607–756) and GST–FIP4 (residues 484–637) as efficiently as with GST–GGA1-GAT, which interacts with all ARF isoforms (19). In contrast, ARF1(Q71L) was pulled down with GST–GGA1-GAT but not with either FIP construct. Thus, our data support and extend the conclusion that FIP3 and FIP4 interact with both ARF5 and ARF6. The discrepancies may reflect differences in the experimental systems used; the Exton group (9, 15), like us, used GST–FIPs to pull down ARFs, whereas the Gould group (13) used GST-ARFs to pull down FIPs. However, a recent paper from the Gould group (18), published while our study was in progress, showed that both FIP3 and FIP4 preferentially bind ARF6 rather than ARF5.

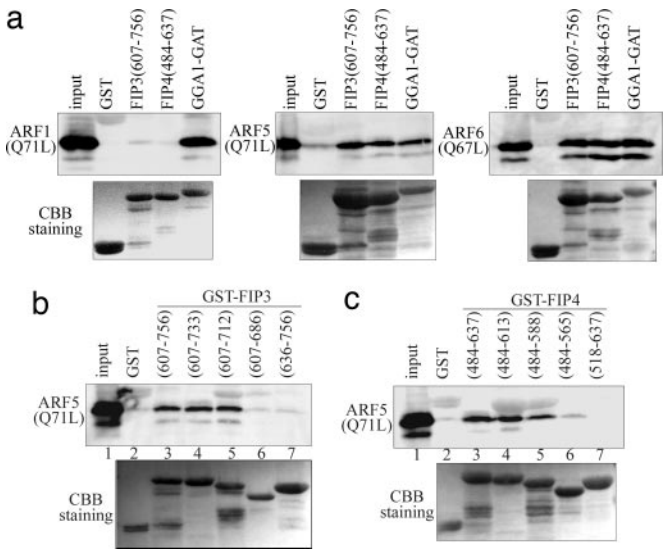

Fig. 2. Specific interactions of FIP3 and FIP4 with ARF5/6 and delineation of the FIP ABD. (*a*) Extracts of HeLa cells expressing HA-tagged ARF1(Q71L) (*Left*), ARF5(Q71L) (*Center*) or ARF6(Q67L) (*Right*) were pulled down with GST or FIP3 (residues 607–756), FIP4 (residues 484–637), or GGA1-GAT fused to GST. (*Upper*) The extracts were then processed for immunoblot analysis to detect bound ARF-HA. (*Lower*) The blots were then stained with CBB. (*b* and *c*) Extracts of HeLa cells expressing HA-ARF5(Q71L) were pulled down with GST or FIP3 (*b*) or FIP4 (*c*) fragments fused to GST as indicated. (*Upper*) The extracts were then processed for immunoblot analysis to detect bound HA-ARF5(Q71L). (*Lower*) The blots were then stained with CBB.

Our preliminary two-hybrid analysis suggested that the RBD of FIP3 or FIP4 was not required for binding ARF (data not shown). We confirmed this observation and further characterized the ABD by pull-down assay. As expected, a FIP3 construct (residues 607–733) lacking the RBD retained the ability to bind ARF5(Q71L) (Fig. 2*b*, lane 4). Truncation of 21 aa from the RBD boundary (residues 607–712) (Fig. 2*b*, lane 5) did not affect ARF5 binding, but a further 26 aa truncation (residues 607–686) (Fig. 2*b*, lane 6) completely abrogated ARF binding. Proceeding from the other direction, truncation of 30 aa from the N terminus of the original construct abolished ARF binding (residues 636–756) (Fig. 2*b*, lane 7). Thus, the ABD of FIP3 is contained within residues 607–712. Using a similar approach, we determined that residues 484–588 encompass the FIP4 ABD (Fig. 2*c*).

Simultaneous Binding of Rab11 and ARF5 to FIP3. Considering the data reported above that the ABD and RBD are distinct, we examined whether FIP3 simultaneously binds Rab11 and ARF5. We incubated a constant amount of GST-Rab11(Q70L) prebound to glutathione-Sepharose beads with a constant amount of His_6/T7-FIP3 and a varying amount of His_6/T7-ARF5(Q71L), and bound material was analyzed by immunoblotting with anti-T7-tag antibody. The amount of His_6/T7-FIP3 and His_6/T7-ARF5(Q71L) pulled down with GST-Rab11(Q70L) was constant irrespective of the amount of His_6/T7-ARF5(Q71L) (Fig. 8, which is published as supporting information on the PNAS web site), suggesting the independent and simultaneous binding of Rab11 and ARF5 to FIP3.

Crystallization of FIP3-RBD in Complex with Rab11. We attempted to crystallize the FIP3 fragment (residues 607–756), which includes both the ABD and RBD (Fig. 7) in complex with a C-terminally truncated form of Rab11(Q70L) (residues 1–173; hereafter called Rab11). However, the obtained cocrystal contained a smaller FIP3 fragment that had undergone partial degradation during the crystallization procedure. Mass spectroscopic analysis and N-terminal sequencing revealed that the obtained crystal contained intact Rab11 and a C-terminal 42-aa fragment (residues 715–756) of FIP3. We therefore prepared this fragment (hereafter called FIP3-RBD) for further cocrystallization studies. Initial phases were determined with selenomethionine (SeMet)-substituted proteins by the multiple anomalous dispersion method, and the structure was refined to 1.75-Å resolution (Table 1, which is published as supporting information on the PNAS web site). The final model includes all amino acids (residues 715–756) of FIP3-RBD and residues 7–173 of Rab11 with a bound GTP molecule and a Mg^{2+} ion.

Overall Structure of the Rab11–FIP3-RBD Complex. The cocrystal contained two Rab11 and two FIP3-RBD molecules in the asymmetric unit (Fig. 3 *a* and *b*). Each FIP3-RBD consists of an N-terminal long α-helix (residues 716–748) followed by a 90° bend at the conserved Pro-750 residue, a 3^{10} helix (residues 750–752), and a C-terminal short β-strand (residues 753–755), adopting an "L" shape (Fig. 9, which is published as supporting information on the PNAS web site). The long α-helix forms a parallel coiled-coil homodimer (Fig. 9) that symmetrically interacts with two Rab11 molecules on both sides, forming a quaternary Rab11–$(FIP3\text{-}RBD)_2$–Rab11 complex (Fig. 3 *a* and *b*). Here we identify molecules in the quaternary complex as "*A*–(*C*–*D*)–*B*"; where *A* and *B* designate Rab11 and *C* and *D* designate FIP3-RBD (Fig. 3*a*). The switch 1, switch 2, and interswitch regions of Rab11 interact with the C-terminal half of the long α-helix and the short β-strand of FIP3-RBD. The Rab11–$(FIP3\text{-}RBD)_2$–Rab11 tetrameric complex is not completely dyad-symmetric, showing remarkable deviations

BIOCHEMISTRY

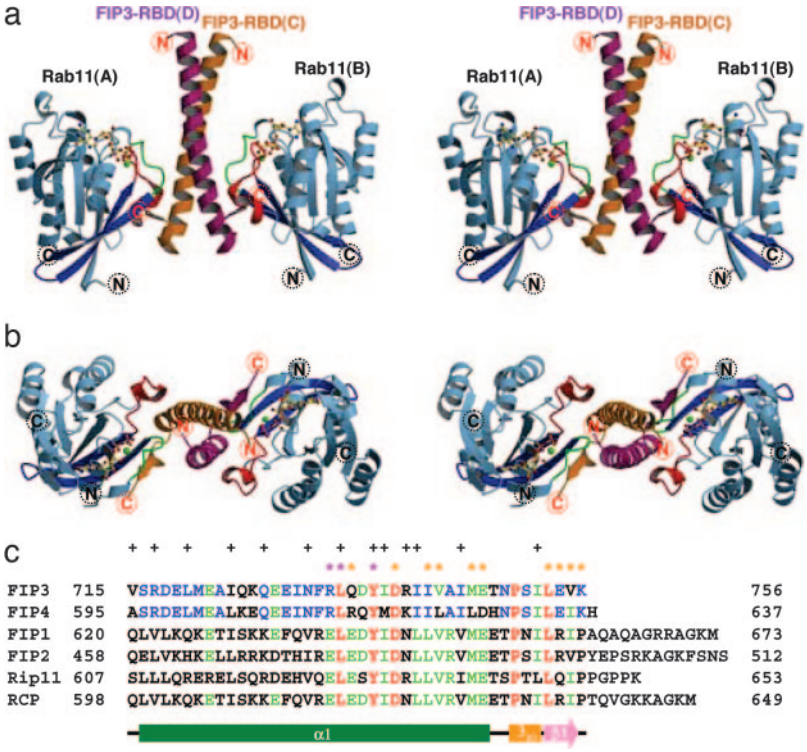

Fig. 3. Structure of the Rab11–FIP3-RBD complex. (*a*) Ribbon stereodiagram of the Rab11–FIP3-RBD complex (side view). The asymmetric unit contains two Rab11 (molecules *A* and *B*) and two FIP3-RBD (molecules *C* and *D*) molecules. The switch 1, switch 2, and interswitch regions of Rab11 are highlighted in green, red, and blue, respectively. GTP and Mg^{2+} ions are shown as ball-and-stick models. Encircled N and C stand for N and C termini, respectively. (*b*) Top view of *a*. (*c*) Sequence alignment of the RBD of the human FIP family proteins. Red, residues identical among all of the members; green, residues conserved among at least four members; blue, residues conserved between FIP3 and FIP4. The secondary structures of FIP3-RBD are schematically shown at the bottom. The residues involved in dimerization are marked with a + symbol. Orange (molecule *C*) and purple (molecule *D*) asterisks above the sequences stand for the residues involved in the interaction with Rab11 (molecule *A*).

in the switch 2 region of Rab11 and the N-terminal region of FIP3-RBD (see below).

FIP3 Homodimer Formation. The homodimerization of FIP3-RBD in the crystal is compatible with the previous observation that FIPs form homodimers in solution (20). The α-helical portion of FIP3-RBD is amphiphilic, as previously predicted (12, 14, 21). The hydrophobic side of the amphiphilic helix mediates formation of the parallel coiled-coil homodimer (Fig. 9) in which the interface is predominantly hydrophobic with several additional hydrogen bonds, burying 964 Å^2 of accessible surface area. The two protomers of the FIP3-RBD homodimer have essentially the same C-terminal structure (residues 733–756; the C^α atom rmsd between the two protomers is 0.12 Å), whereas the helical axes of the N-terminal half of the two protomers (residues 715–732) tilt ≈20° toward each other when the C-terminal half of the protomers are superimposed. It is possible that the asymmetric distortion of the α-helices was caused by nonphysiological contacts between the N terminus of the FIP3-RBD α-helix and the neighboring Rab molecule in the crystal.

Rab11 Structure. GTP-bound Rab11 contains six β-strands (β1–β6) and five α-helices (α1–α5) like other Rab GTPases. The rmsd between Rab11-GTP (molecule A) in complex with FIP3-RBD and free Rab11-GTP (22) [Protein Data Bank (PDB) ID code 1OIW] is 1.09 Å for all C^α atoms, but the value drops to 0.39 Å if switch 1 and switch 2 are excluded from the comparison (Fig. 10, which is published as supporting information on the PNAS web site). In particular, the switch 2 conformation differs substantially between free Rab11-GTP and Rab11-GTP complexed with FIP3-RBD (Fig. 4). In the free Rab11-GTP structure, the switch 2 region is not helical and makes only limited interactions with switch 1 (22). When complexed with FIP3-RBD, however, switch 2 is farther away from switch 1 to accommodate the FIP3-RBD α-helix between these switch regions (Fig. 4). Furthermore, the switch 2 regions of the two Rab11 molecules in the complex take somewhat different conformations (Fig. 4); the flexibility of switch 2 is suggested by its large *B* factors and poor electron density.

FIP3–Rab11 Interaction. In the quaternary Rab11–$(FIP3\text{-}RBD)_2$–Rab11 complex, the Rab11-interacting region of FIP3-RBD is confined to the C-terminal 24 aa (residues 733–756), which cover the C-terminal half of the long α-helix and the short β-strand (Fig. 3*c*); this region corresponds well with the Rab11-binding domain determined biochemically (11, 14) (Fig. 1*a*). Rab11 recognition by FIP3-RBD is essentially the same between the two symmetric interfaces, and the interaction between Rab11 and FIP3-RBD buries accessible surface areas of 771 and 737 Å^2 from Rab11 molecules *A* and *B*, respectively. Binding to FIP3-RBD involves three regions of Rab11: (*i*) switch 1, (*ii*) switch 2, and (*iii*) interswitch (Fig. 11, which is published as supporting information on the PNAS web site).

Switch 1. Although the amphiphilic α-helix of FIP3-RBD is responsible for homodimerization on its hydrophobic side [*C–D* interaction in the quaternary *A*–(*C–D*)–*B* complex] (Fig. 9), the same side

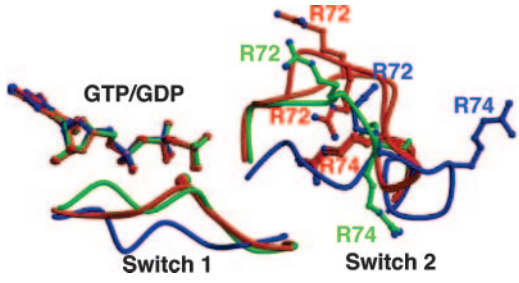

Fig. 4. Superposition of Rab11 in different forms. The switch 1 and switch 2 regions are shown. The side chains of Arg-72 and Arg-74 in the switch 2 region are indicated by ball-and-stick models. GTP/GDP molecules also are presented as ball-and-stick models. The GDP-bound form (PDB ID code 1OIV) is blue, the GTP-bound free form (PDB ID code 1OIW) is green, and molecule *A* GTP-bound Rab11 in complex with FIP3-RBD is red, whereas molecule *B* is orange.

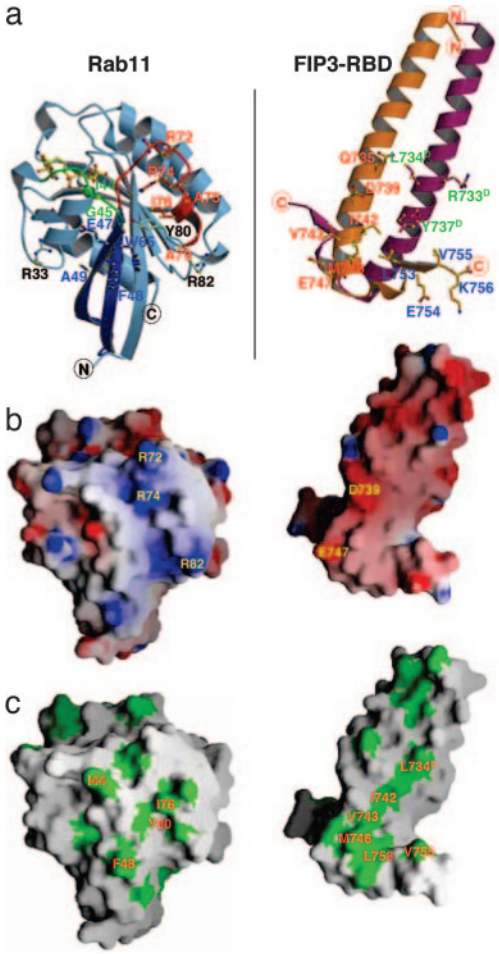

Fig. 5. Interface between Rab11 and FIP3-RBD. (*a*) The Rab11 and FIP3-RBD interface in an ''open book'' representation. (*Left*) Rab11 (molecule *A*) is shown as a ribbon diagram. (*Right*) The FIP3-RBD dimer. The color scheme is the same as that of Fig. 3*b*. The residues involved in the interactions are displayed as ball-and-stick models. (*b*) Molecular surface representation of *a*. The surfaces are colored according to the electrostatic surface potential (blue, positive; red, negative; scale, -10 to $+10$ kTe^{-1}). (*c*) The hydrophobicity is green and is shown in the same view as *a*.

in the middle of the α-helix also is involved in binding the switch 1 region of the Rab11 molecule (*A–D* and *B–C* interactions) (Figs. 3 and 5). The interaction is hydrophobic in nature (Fig. 5*c*), with the Tyr-737 side chain of FIP3-RBD packing against the Ile-44 side chain and Gly-45 of Rab11 and the side chain of Leu-734 and the aliphatic portion of the Arg-733 side chain interacting with the side chain of Ile-44 in the Rab11 switch 1 region (Fig. 6*a*).

Switch 2. The hydrophilic side of the amphiphilic helix of FIP3-RBD, which is opposite the dimer interface, faces switch 2 of the other Rab11 molecule (*A–C* and *B–D* interactions) (Figs. 3 and 5). In addition to hydrophilic residues (Gln-735, Asp-736, Asp-739, Arg-740, and Glu-747), the hydrophilic side includes the hydrophobic residues Val-743 and Met-746 (Figs. 5 and 6*b*). The hydrophilic interaction of Rab11 with FIP3-RBD involves features unique to its switch 2, which is largely disordered and less helical compared with those of other Rabs (22) (Fig. 5*a*). The side chains of Arg-74 and Arg-82 in the disordered switch 2 form salt bridges with Asp-739 and Glu-747, respectively (Figs. 5*b* and 6*b*). In addition, the side chain of Arg-72 in the switch 2 loop forms a hydrogen bond with the Gln-735 side chain (Fig. 6*b*), although only at the *A–C* interface. Another remarkable feature of Rab11 switch 2 is that the side chain of Tyr-80, one of three invariant hydrophobic residues in the Rab family (23), points inward (Fig. 6*b*), thereby forming an intramolecular hydrogen bond with the main chain carbonyl of Leu-16. In striking contrast, the side chain of the corresponding Tyr/Phe residue points outward in all of the reported structures of GTP-bound Rab proteins, except Rab11 and Rab7/Ypt7. As a result, Rab11 forms a characteristic, large hydrophobic pocket surrounded by Ile-76, Ala-79, and Tyr-80 of switch 2; Trp-65 of the interswitch region; and Val-46 of switch 1 (Figs. 5 *a* and *c*), which accommodates the large side chain of FIP3-RBD Met-746 (Fig. 6*b*). Furthermore, at the top of this pocket, Ala-75 and Ile-76 come in hydrophobic contact with Val-743 and Ile-742, respectively, of FIP3-RBD (Fig. 6*b*).

Interswitch. Finally, an intermolecular parallel β-sheet is formed between the C-terminal short β-strand of FIP3-RBD and the β3-strand of the Rab11 interswitch region (*A–C* and *B–D* interactions) (Figs. 3 and 6*c*); the main chains of Leu-753 (carbonyl oxygen) and Val-755 (amide nitrogen) of FIP3-RBD form hydrogen bonds with the main chain of Phe-48 (amide nitrogen and carbonyl oxygen) of Rab11.

Mutational Experiments. Residues involved in the Rab11 interaction are well conserved in the FIP family (Fig. 3*c*). To validate the structurally observed molecular interactions, we mutated FIP3 residues expected to be critical for its interaction with Rab11. All of the mutations examined abolished the binding of GST–FIP3 (residues 607–756) to Rab11(Q70L) (Fig. 12, which is published as supporting information on the PNAS web site). The Y737S mutation abolished Rab11 binding, indicating the importance of the Tyr residue in mediating the interaction with Rab11 switch 1 (Fig. 6*a*). Furthermore, the loss of the Rab11 binding when either Asp-739 or Glu-747 were mutated to Ala indicates the importance of the salt bridges formed by these residues with the Rab11 switch 2 region. In addition, the inability of M746S to bind Rab11 verifies the importance of this hydrophobic residue in filling the large hydrophobic pocket involving the Rab11 switch 2 region (Fig. 6*b*). Finally, FIP3 (residues 607–752) is unable to bind Rab11, confirming that the C-terminal β-strand is essential for intermolecular β-sheet formation with the Rab11 interswitch region (Fig. 6*c*).

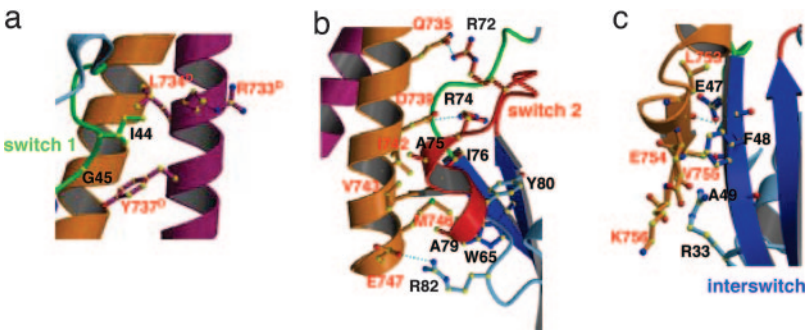

Fig. 6. Interaction between Rab11 and FIP3-RBD. Shown are close-up views of the switch 1 (*a*), switch 2 (*b*), and interswitch (*c*) regions of Rab11 in complex with FIP3-RBD. The color scheme is the same as that of Fig. 3*b*. Residues involved in the interaction are labeled and indicated by ball-and-stick models. The cyan dashed lines indicate hydrogen bonds or electrostatic interactions.

Discussion

Specificity of Rab11–FIP3-RBD Interaction. We examined the structural basis for the specific recognition of Rab11 by FIPs in detail. FIPs form homodimers in solution, and the obtained Rab11–$(FIP3\text{-}RBD)_2$–Rab11 structure supports these data (20, 24). Additionally, our structural data confirm that the RBD of FIPs adopt an amphiphilic helical conformation (12, 14, 21). The FIP3-RBD homodimer interacts with the switch 1, switch 2, and interswitch regions of Rab11, and, although the RabSF1–RabSF4 regions (25) also are involved in effector recognition in several Rab–effector complexes, this is not the case with the Rab11–FIP3-RBD complex. Rab11 switch 2 structure is unique among Rab family members and is essential for its specific interaction with FIP3-RBD independent of the RabSF regions. In particular, the side chain of Tyr-80, one of the three invariant aromatic residues in the Rab family, points inward to form a large hydrophobic pocket together with switch 1 to accommodate the FIP3-RBD. In contrast, the side chain of the corresponding aromatic residue in other GTP-bound Rab proteins generally points toward the solvent (26), except for Rab7 (PDB ID code 1VG8) and Ypt7 (PDB ID code 1KY2). Rab7/Ypt7, however, cannot bind FIP3-RBD because of the tight interactions between the two switch regions.

In other Rab–effector and ARF–effector complexes, one particular effector residue typically located close to the conserved Gly residue of switch 1 (Gly-45 in Rab11), generally plays a crucial role in recognizing switch 1 and switch 2 of the GTPases in their GTP-bound state (27). In the case of FIP3-RBD, however, the corresponding residue, Ile-742, has a limited interaction with the poorly ordered switch 2 region of Rab11; instead, Asp-739 and Met-746 appear to participate in the Rab11 interaction (Fig. 6*b*).

We observed dyad-symmetric binding in the Rab11–FIP3-RBD complex, and several other GTPase–effector complexes adopt similar binding modes, including Rab5–Rabaptin-5 (28), Rab7–RILP (29), and Arl1–GRIP (30, 31). However, the relative orientation of the effector to the GTPase molecule in these complexes differs substantially from the Rab11–FIP3-RBD complex. Detailed structural comparisons are described in *Supporting Text* and Figs. 13 and 14, which are published as supporting information on the PNAS web site.

Mutational Analyses of Rab11–FIP-RBD Interaction. The structure of the Rab11–FIP3-RBD complex is consistent with current and previous studies using FIP mutants.

Mutations of switch 1-interacting residues. The Y737S mutant of FIP3 (Fig. 12) and the corresponding Y629A mutant of Rip11 (reported in ref. 20 as Y628A) do not bind Rab11, but the Rip11 Y629F mutant and the RCP Y620F mutant retain their Rab-binding ability (21), highlighting the importance of the hydrophobic portion of this conserved Tyr residue in supporting FIP interactions with switch 1 (Fig. 6*a*).

Mutations of switch 2-interacting residues. The D739A and E747A mutants of FIP3 (Fig. 12) and the D619A FIP4 mutant (reported in ref. 18 as D538A) also fail to bind Rab11. We propose that neutralization of these acidic residues disrupts the two salt bridges between switch 2 of Rab11 and these residues on the hydrophilic side of the amphiphilic RBD helix (Figs. 5*b* and 6*b*). In contrast, mutation of the corresponding Asp-631 or Glu-639 residues of Rip11 to Ala (20) or Asp-622 to Asn of RCP (21) does not affect Rab11 binding. Interestingly, FIP3 has a Gln residue at position 735, and Rip11 and RCP have a Glu residue at the corresponding position (Fig. 3*c*). FIP3 Gln-735 forms a hydrogen bond with Arg-72 of Rab11 switch 2 (Fig. 6*b*), and a substituted Glu residue at this position may form a third salt bridge with Arg-72 of Rab11, thereby overcoming the loss of one of the other two salt bridges in the Rab11–Rip11 and Rab11–RCP interactions. On the other hand, mutation of Met-746 to Ser in FIP3 abolishes Rab11 binding (Fig. 12), supporting the structural data that this hydrophobic residue is required to fill the large pocket characteristic of Rab11 (Fig. 6*b*).

Mutations of interswitch-interacting residues. The FIP3 fragment (residues 607–752) does not bind Rab11 (Fig. 12), suggesting that the C-terminal β-strand is essential for intermolecular β-sheet formation (Fig. 6*c*).

Mutations of residues involved in RBD dimerization. Ile-738 of FIP3 is located at the dimerization interface and interacts with the side chains of Leu-734 and Tyr-737 of the counterpart molecule (Fig. 9). Although Ile-738 is not in direct contact with Rab11, the I738E mutation abolishes Rab11 binding and endosomal targeting of FIP3 (17, 18). Moreover, the corresponding I630E mutation of Rip11 disrupts Rab11 binding, whereas the conservative substitution I630V has no effect on Rab11 binding (14, 20). Furthermore, the RCP I621E mutant does not dimerize, bind Rab11, or associate with endosomal membranes (21). Taken together, all of these data support our structural data that dimerization of the RBD is essential for Rab11 binding.

Dual Interaction of Class II FIPs with ARF and Rab11. In this study, we showed that FIP3 and FIP4 have distinct binding regions for Rab11 and ARF5/ARF6 and can bind simultaneously to these GTPases. The predicted long α-helical structure of the region containing both RBD and ABD (14, 24) makes it possible that the ABD projects away from the Rab11-positive membrane. This possibility leads to a model wherein the Rab11-positive vesicles are tethered to the ARF5/ARF6-positive compartments by virtue of FIP3/FIP4, leading to membrane fusion. Alternatively, the ABD may lie along the Rab11-positive membrane. In this case, FIP3/FIP4 links Rab11- and ARF5/ARF6-positive microdomains within the same compartment, thereby triggering ARF-mediated vesicle budding. Determining the crystal structure of the triple Rab11–FIP–ARF complex will provide invaluable insight into the mechanism underlying the vesicle delivery, although our attempts so far have been unsuccessful because of the extreme instability of constructs containing the ABD.

Methods

Pull-Down Assays. Bacterial expression vectors for GST fusion and His_6/T7-tagged proteins were constructed by subcloning cDNA fragments into pGEX-6P1 (GE Healthcare, Bucks, U.K.) and pET28a (Novagen, Darmstadt, Germany), respectively. Mammalian expression vectors for HA-tagged human Rab11a(Q70L), FIP3, and FIP4 were constructed by subcloning the corresponding cDNA fragments into pcDNA3-HAN (32). Construction of expression vectors for HA-tagged ARFs was described previously (19, 33, 34).

GST fusion proteins of human FIP3 or FIP4 mutants were expressed in *Escherichia coli* BL21(DE3) cells and purified with glutathione-Sepharose 4B beads (GE Healthcare). HeLa cell lysates expressing HA-Rab11a(Q70L), ARF1(Q71L)-HA, ARF5(Q71L)-HA, or ARF6(Q67L)-HA were prepared as follows. Twelve hours after transfection of the Rab11 or ARF vector, the cells were lysed in buffer A (20 mM Tris·HCl, pH 7.4/100 mM NaCl/2 mM $MgCl_2$/1% Triton X-100/10% glycerol) containing a protease inhibitor mixture (Complete EDTA-free, Roche Diagnostics, Basel, Switzerland) and 100 μM GTP-γS. The lysate supernatant was precleared with glutathione-Sepharose 4B beads and incubated for 1 h at 4°C with the GST–FIP3 or GST–FIP4 protein, or GST–GGA1-GAT (19, 34), prebound to glutathione-Sepharose 4B beads. The beads were then pelleted and washed four times with buffer B (buffer A containing 1% Nonidet P-40 instead of 1% Triton X-100). The bound materials were processed for immunoblotting using the monoclonal anti-HA antibody (Roche Diagnostics), peroxidase-conjugated secondary antibody, and ECL reagents (GE Healthcare).

The simultaneous interaction of ARF5 and Rab11 with FIP3 was examined as follows. His_6/T7-FIP3 and His_6/T7-Δ12ARF5(Q71L)

were expressed in BL21(DE3) cells and purified with a Probond resin (Invitrogen, Carlsbad, CA). GST-Rab11a(Q70L) prebound to glutathione-Sepharose 4B beads was incubated with His_6/T7-FIP3 and His_6/T7-Δ12ARF5(Q71L) in buffer A for 1 h at 4°C. The materials bound to the beads were processed for immunoblotting using the monoclonal anti-T7 tag antibody (Novagen) as described above.

Protein Expression, Purification, and Crystallization. For crystallization of Rab11a(Q70L), a cDNA fragment encoding a truncated protein lacking the C-terminal 43 aa, Rab11aΔC43(Q70L), was subcloned into pGEX-6P1. Cells expressing GST-Rab11aΔC43(Q70L) or GST-FIP3 (residues 607–756) were harvested after induction with 1 mM isopropyl β-D-thiogalactoside for 6 h at 25°C and lysed in PBS by sonication. The lysate supernatant was loaded on a glutathione-Sepharose 4B column. GST-Rab11aΔC43(Q70L) was eluted with glutathione and cleaved with PreScission protease (GE Healthcare). The protein was purified by Superdex 75 chromatography in buffer C (20 mM Tris·HCl, pH 8.0/100 mM NaCl/5 mM $MgCl_2$). The purified Rab11aΔC43(Q70L) was added to GST–FIP3 (residues 607–756) and cleaved with PreScission protease. The complex was purified by Superdex 75 chromatography in buffer C. We obtained crystals of the complex, but FIP3 underwent partial degradation. Mass spectroscopic analysis and N-terminal sequencing of the resulting crystals revealed that they contained a C-terminal fragment of FIP3 (residues 715–756) and Rab11aΔC43(Q70L). We therefore subcloned the cDNA fragment for FIP3 (715–756) (FIP3-RBD) and used it for cocrystallization with Rab11aΔC43(Q70L). SeMet-substituted Rab11ΔC43(Q70L) and FIP3-RBD were expressed in *E. coli* DL41 cells and purified by the same procedures as described above. The SeMet-substituted Rab11–FIP3-RBD complex was concentrated to ≈5.0 $mg \cdot ml^{-1}$ with buffer C. Crystallization conditions for the native and SeMet-substituted Rab11–FIP3-RBD complexes were screened by using the hanging drop vapor diffusion method at 289 K. Crystals were obtained after 5 days against a reservoir containing 20% isopropanol, 3–5% (wt/vol) PEG 4000, and 0.05 M MES-NaOH, pH 5.8–6.0.

X-Ray Data Collection and Processing. The crystals of the SeMet-substituted Rab11–FIP3-RBD complex were picked from the droplets with cryo-loops, transferred to mother liquor solution containing an additional 15% glycerol, and then flash-frozen in liquid nitrogen. For crystal structure analysis, the multiple anomalous dispersion data set was collected to 2.25-Å resolution at 100 K with synchrotron radiation at beamline 6A of the Photon Factory at the High Energy Accelerator Research Organization. A single wavelength data set with another SeMet crystal was collected to a higher resolution of 1.75 Å at beamline PF-AR NW12A. The crystals belong to the orthorhombic space group $P2_12_12$ with unit-cell dimensions $a = 108.7$, $b = 120.6$, and $c = 36.2$ Å. Data were processed with HKL2000 (35). The data collection and processing statistics are summarized in Table 1.

Structure Determination and Refinement. The crystal structure of the Rab11–FIP3-RBD complex was solved by using the multiple anomalous dispersion method. The program SOLVE (36) was used to locate and refine six of the eight Se sites. The RESOLVE (37) program was used for solvent flattening, assuming a 47% solvent content. The initial electron density map at the Rab11–FIP3-RBD complex region was very clear after solvent flattening. An initial model was generated with RESOLVE and refined with CNS (38), and model building was carried out with TURBO-FRODO (39). The final model refined for the resolution range from 40.0 to 1.75 Å has an R factor of 20.2% and an R_{free} of 22.3%. The final model includes two Rab11 (residues 7–173), two FIP3-RBD, two GTP molecules, two Mg^{2+} ions, one MES molecule, and 419 water molecules, and it has excellent geometry, with no Ramachandran outliers in disallowed regions (most favored region, 93.0%; additionally allowed region, 7.0%). The final refinement statistics are shown in Table 1. Figures were produced with MOLSCRIPT (40), Raster3D (41), and POVScript+ (42).

This work was supported in part from the Ministry of Education, Culture, Sports, Science, and Technology of Japan; the Japan Society for Promotion of Science; the Protein 3000 Project; the Naito Foundation; the Takeda Science Foundation; and the Novartis Foundation of Japan. H.K. was supported as a research assistant by the 21st Century Center of Excellence Program "Knowledge Information Infrastructure for Genome Science" and as a research fellow by the Japan Society for Promotion of Science for Japanese Junior Scientists.

1. Chavrier P, Goud B (1999) *Curr Opin Cell Biol* 11:466–475.
2. Moss J, Vaughan M (1995) *J Biol Chem* 270:12327–12330.
3. Donaldson JG (2003) *J Biol Chem* 278:41573–41576.
4. Zerial M, McBride H (2001) *Nature Rev Mol Cell Biol* 2:107–117.
5. Urbé S, Huber LA, Zerial M, Tooze SA, Parton RG (1993) *FEBS Lett* 334:175–182.
6. Ullrich O, Reinsch S, Urbe S, Zerial M, Parton RG (1996) *J Cell Biol* 135:913–924.
7. Ren M, Xu G, Zeng J, De Lemos-Chiarandini C, Adesnik M, Sabatini DD (1998) *Proc Natl Acad Sci USA* 95:6187–6192.
8. Wilcke M, Johannes L, Galli T, Mayau V, Goud B, Salamero J (2000) *J Cell Biol* 151:1207–1220.
9. Shin OH, Ross AH, Mihai I, Exton JH (1999) *J Biol Chem* 274:36609–36615.
10. Prekeris R, Klumperman J, Scheller RH (2000) *Mol Cell* 6:1437–1448.
11. Prekeris R, Davies JM, Scheller RH (2001) *J Biol Chem* 276:38966–38970.
12. Hales CM, Griner R, Hobdy-Henderson KC, Dorn MC, Hardy D, Kumar R, Navarre J, Chan EK, Lapierre LA, Goldenring JR (2001) *J Biol Chem* 276:39067–39075.
13. Hickson GR, Matheson J, Riggs B, Maier VH, Fielding AB, Prekeris R, Sullivan W, Barr FA, Gould GW (2003) *Mol Biol Cell* 14:2908–2920.
14. Meyers JM, Prekeris R (2002) *J Biol Chem* 277:49003–49010.
15. Shin OH, Couvillon AD, Exton JH (2001) *Biochemistry* 40:10846–10852.
16. Horgan CP, Walsh M, Zurawski TH, McCaffrey MW (2004) *Biochem Biophys Res Commun* 319:83–94.
17. Wilson GM, Fielding AB, Simon GC, Yu X, Andrews PD, Hames RS, Frey AM, Peden AA, Gould GW, Prekeris R (2005) *Mol Biol Cell* 16:849–860.
18. Fielding AB, Schonteich E, Matheson J, Wilson G, Yu X, Hickson GR, Srivastava S, Baldwin SA, Prekeris R, Gould GW (2005) *EMBO J* 24:3389–3399.
19. Takatsu H, Yoshino K, Toda K, Nakayama K (2002) *Biochem J* 365:369–378.
20. Junutula JR, Schonteich E, Wilson GM, Peden AA, Scheller RH, Prekeris R (2004) *J Biol Chem* 279:33430–33437.
21. Lindsay AJ, McCaffrey MW (2004) *FEBS Lett* 571:86–92.
22. Pasqualato S, Senic-Matuglia F, Renault L, Goud B, Salamero J, Cherfils J (2004) *J Biol Chem* 279:11480–11488.
23. Merithew E, Hatherly S, Dumas JJ, Lawe DC, Heller-Harrison R, Lambright DG (2001) *J Biol Chem* 276:13982–13988.
24. Wallace DM, Lindsay AJ, Hendrick AG, McCaffrey MW (2002) *Biochem Biophys Res Commun* 292:909–915.
25. Pereira-Leal JB, Seabra MC (2000) *J Mol Biol* 301:1077–1087.
26. Eathiraj S, Pan X, Ritacco C, Lambright DG (2005) *Nature* 436:415–419.
27. Kawasaki M, Nakayama K, Wakatsuki S (2005) *Curr Opin Struct Biol* 15: 681–689.
28. Zhu G, Zhai P, Liu J, Terzyan S, Li G, Zhang XC (2004) *Nat Struct Mol Biol* 11:975–983.
29. Wu M, Wang T, Loh E, Hong W, Song H (2005) *EMBO J* 24:1491–1501.
30. Panic B, Perisic O, Veprintsev DB, Williams RL, Munro S (2003) *Mol Cell* 12:863–874.
31. Wu M, Lu L, Hong W, Song H (2004) *Nat Struct Mol Biol* 11:86–94.
32. Shin H-W, Shinotsuka C, Torii S, Murakami K, Nakayama K (1997) *J Biochem* 122:525–530.
33. Hosaka M, Toda K, Takatsu H, Torii S, Murakami K, Nakayama K (1996) *J Biochem* 120:813–819.
34. Shin, H-W, Morinaga N, Noda M, Nakayama K (2004) *Mol Biol Cell* 15:5283–5294.
35. Otwinowski Z, Minor W (1997) *Methods Enzymol* 276:307–326.
36. Terwilliger TC, Berendzen J (1999) *Acta Crystallogr D* 55:849–861.
37. Terwilliger TC (2003) *Acta Crystallogr D* 59:38–44.
38. Brünger AT, Adams PD, Clore GM, DeLano WL, Gros P, Grosse-Kunstleve RW, Jiang JS, Kuszewski J, Nilges M, Pannu NS, *et al.* (1998) *Acta Crystallogr D* 54:905–921.
39. Roussel A, Cambilleau C (1989) *Turbo-Frodo* (Silicon Graphics, Mountain View, CA).
40. Kraulis PJ (1991) *J Appl Crystallogr* 24:946–950.
41. Merritt EA, Murphy M (1994) *Acta Crystallogr D* 50:869–873.
42. Fenn TD, Ringe D, Petsko GA (2003) *J Appl Cryst* 36:944–947.